



HAL
open science

A Paleozoic age for the Tunnunik impact structure

Camille Lepaulard, Jérôme Gattacceca, Nicholas Swanson-Hysell, Yoann Quesnel, François Demory, Gordon Osinski

► **To cite this version:**

Camille Lepaulard, Jérôme Gattacceca, Nicholas Swanson-Hysell, Yoann Quesnel, François Demory, et al.. A Paleozoic age for the Tunnunik impact structure. *Meteoritics and Planetary Science*, 2019, 54 (4), pp.740-751. 10.1111/maps.13239 . hal-02048190

HAL Id: hal-02048190

<https://hal.science/hal-02048190>

Submitted on 26 Apr 2019

HAL is a multi-disciplinary open access archive for the deposit and dissemination of scientific research documents, whether they are published or not. The documents may come from teaching and research institutions in France or abroad, or from public or private research centers.

L'archive ouverte pluridisciplinaire **HAL**, est destinée au dépôt et à la diffusion de documents scientifiques de niveau recherche, publiés ou non, émanant des établissements d'enseignement et de recherche français ou étrangers, des laboratoires publics ou privés.

1
2 **A Paleozoic age for the Tunnunik impact structure**
3

4 **Camille Lepaulard¹, Jérôme Gattacceca¹, Nicholas Swanson-Hysell², Yoann Quesnel¹,**
5 **François Demory¹, Gordon R. Osinski^{3,4},**
6

7 ¹Aix Marseille Univ, CNRS, IRD, Coll France, INRA, CEREGE, Aix-en-Provence, France

8 ² Department of Earth and Planetary Science, University of California, Berkeley, California
9 94720-4767, USA

10 ³ Dept. of Earth Sciences, Centre for Planetary Science and Exploration, University of Western
11 Ontario, 1151 Richmond St., London, ON, N6A 5B7, Canada

12 ⁴Dept. Physics & Astronomy, University of Western Ontario, 1151 Richmond St., London, ON,
13 N6A 5B7, Canada

14
15 Corresponding author: Camille Lepaulard (lepaulard@cerege.fr)

16 **Key Points:**

- 17
- The Tunnunik impact structure is most likely to have formed in the Late Ordovician to early Silurian
 - The post-impact temperature of the studied target sedimentary rocks was about 350°C
- 18
19

20 Abstract

21 We report paleomagnetic directions from the target rocks of the Tunnunik impact
22 structure, as well as from lithic impact breccia dikes that formed during the impact event. The
23 target sedimentary rocks have been remagnetized after impact-related tilting during a reverse
24 polarity interval. Their magnetization is unblocked up to 350°C. The diabase dikes intruding
25 these sediments retained their original magnetization which unblocks above 400°C. The impact
26 breccia records a paleomagnetic direction similar to that of the overprints in the target
27 sedimentary rocks. The comparison of the resulting virtual geomagnetic pole for the Tunnunik
28 impact structure with the apparent polar wander path for Laurentia combined with
29 biostratigraphic constraints from the target sedimentary rocks is most consistent with an impact
30 age in the Late Ordovician or Silurian, around 430 to 450 Ma, soon after the deposition of the
31 youngest impacted sedimentary rocks. Our results from the overprinted sedimentary rocks and
32 diabase dikes imply that the post-impact temperature of the studied rocks was about 350°C.

33 34 1 Introduction

35
36 Hypervelocity impacts are a major process for the evolution of planetary surfaces,
37 including the Earth. Terrestrial impact events have significantly influenced the biosphere in
38 numerous ways including, on one hand, the development of habitats for primitive life forms
39 (*Reimold and Koeberl, 2008; Cockell et al., 2005*) and, on the other hand, some extinctions such
40 as the Cretaceous-Paleogene mass extinction (*Schulte et al., 2010*). Depending on the size of the
41 impactor, impact events significantly modify regional geology and may lead to the formation of
42 ore deposits (*Ames et al., 1998*). However, on Earth, plate tectonics and erosion can obscure or
43 completely erase the geologic record of impact structures. Currently, around 190 impact
44 structures are identified on Earth, including thirty in Canada, but the age of approximately half of
45 these impacts is unknown (*Jourdan et al., 2012*). Dating of impact structures is crucial for
46 assessing correlations (or the lack thereof) between impact events and biological or geological
47 changes, and to constrain the flux of crater-forming bodies to the Earth through time.

48 While most of the large terrestrial impact structures (> 6 km) on Earth have likely already
49 been documented (*Hergarten and Kenkmann, 2015*), discovery of additional impact structures is
50 still possible. In 2010, the Tunnunik structure, a ~28 km diameter impact structure was identified
51 in the Canadian Arctic (*Dewing et al., 2013*). The age of this structure is presently not
52 constrained more precisely than between 0 and *ca.* 450 Ma. The purpose of this study is to
53 provide a refined estimate for the age of this impact structure. In the absence of suitable material
54 for radiometric dating, we utilize paleomagnetic dating of target rocks that were remagnetized by
55 the impact (*Deutsch and Schärer, 1994; Pilkington and Grieve, 1992*) and of the lithic breccia
56 that formed during the impact event (*Fairchild et al., 2015*).

57 2 Geological setting, sampling, methods

58 *Geological setting*

59 The Tunnunik impact structure is located on Victoria Island in the Canadian High Arctic.
60 The impact structure is deeply eroded and has been identified by the presence of shatter cones,
61 sedimentary rocks steeply dipping quaquaversally (compared to the generally relatively flat
62 regional bedding), and concentric faults (*Dewing et al., 2013*). The target rock sequence, exposed
63 outside of the impact structure, consists of sub-horizontal sedimentary rocks, mostly dolostones

64 and mudstones, ranging from the Neoproterozoic (Wynniatt formation of the Shaler Supergroup
65 formation) to the Late Ordovician - Early Silurian (?) (Thumb Mountain and Allen Bay
66 formations). Following Newman and Osinski (2016), we group these sedimentary rocks into the
67 Shaler Supergroup (Neoproterozoic), Mount Phayre, Victoria Island, Thumb Mountain and Allen
68 Bay formations in ascending stratigraphic order.

69 Neoproterozoic diabase dikes associated with the *ca.* 720 Ma Franklin Large Igneous
70 Province which intrude the Neoproterozoic sedimentary rocks are also present within the target
71 rock (Dewing *et al.*, 2013; Heaman *et al.* 1992). Lithic impact breccias, composed of
72 sedimentary clasts up to centimeter size set in a silt-sized matrix, are encountered in the form of
73 dikes and sills up to a few decimeters thick intruding the sedimentary target rocks, especially the
74 Mount Phayre formation and the Shaler Supergroup formation.

75 **Sampling**

76 Three main rock types were sampled for paleomagnetic analysis: impact breccia,
77 Neoproterozoic to Upper Ordovician-lower Silurian sedimentary rocks, and Neoproterozoic
78 diabase dikes. For impact breccia sampling, we focused on facies dominated by the fine-grained
79 matrix (clast content below 10 vol%) and with clast size below 1 mm. A total of 29
80 paleomagnetic sites were sampled, mostly located inside the impact structure (Figure 1, Table
81 S1). Sampling was performed by drilling of 2.5 cm-diameter cores using a gas-powered drill, or
82 more rarely through collection of oriented blocks. Samples were oriented using magnetic and sun
83 compasses.

84 **Methods**

85 The magnetic mineralogy was studied by measurement of susceptibility versus
86 temperature (Figure 2A), stepwise thermal demagnetization of saturation isothermal remanent
87 magnetization (sIRM) that is more sensitive to the presence of pyrrhotite (Figure 2B), and
88 measurements of S_{300} ratio that is the IRM obtained after applying a 3 T field and then a back
89 field of -0.3 T normalized to the IRM acquired in 3 T. The low field magnetic susceptibility
90 (noted χ in $\text{m}^3\cdot\text{kg}^{-1}$) was measured for all samples using an AGICO apparatus, either with an
91 MFK1 or a KLY-2 kappabridge instrument (with sensitivity of 5×10^{-13} m^3), depending on sample
92 size. The MFK1 kappabridge operates at 200 Am^{-1} peak field and at a frequency of 976 Hz. The
93 KLY-2 kappabridge operates at 425 Am^{-1} peak field and at a frequency of 920 Hz.
94 Thermomagnetic curves were obtained with the use of the MFK1 instrument coupled with a CS3
95 furnace. Estimates of Curie temperatures were computed as the inflection points of the
96 susceptibility versus temperature curves. Thermal demagnetization of sIRM (imparted with 3 T
97 pulse with a MPM9 pulse magnetizer) was conducted using an MMTD furnace. Hysteresis
98 properties of the diabase dikes were measured with a MicroMag 3900 vibrating sample
99 magnetometer. All rock magnetism measurements were performed at CEREGE.

100 All remanence measurements were performed with a SQUID magnetometer (2G
101 Enterprises, model 760R, with noise level of 10^{-11} Am^2) in a magnetically shielded room, with an
102 attached automated 3-axis alternating field degausser system (with a maximum peak field of 170
103 mT). For the majority of samples, the natural remanence was studied (around 100 specimens) by
104 stepwise thermal demagnetization using a MMTD80 furnace. For each studied site, two pilot
105 samples were demagnetized, one using thermal demagnetization up to 600°C , one using
106 alternating field (AF) demagnetization up to 120 mT. The most efficient demagnetization
107 method was then used for the remaining samples. Demagnetization data were analyzed through

108 principal component analysis and summarized with Fisher statistics using PaleoMac software
109 (*Cogné*, 2003). Paleomagnetic results are summarized in Table 1.

110

111

112 **3 Results**

113

114 In the impact breccia, thermomagnetic experiments reveal a Curie temperature of 585°C,
115 indicating the presence of magnetite (Figure 2A). Pyrrhotite is also present as indicated by
116 significant unblocking of sIRM around 280-320°C (Figure 2B), although its signal is hidden by
117 the magnetite contribution in the susceptibility curve (Figure 2A). The presence of pyrrhotite is
118 confirmed by the S_{-300} ratio of -0.84 that indicates the significant contribution of a high
119 coercivity mineral. The impact breccia samples display two magnetization components that are
120 equally evidenced by thermal (Figure 3A) and AF demagnetization (Figure 3B). The low-
121 temperature/low-coercivity component corresponds to the present local field. The high-
122 temperature (isolated above ~200-350°C and up to the Curie temperature of magnetite at 585°C),
123 high-coercivity (above 15 mT) component is origin-trending and is interpreted as the
124 characteristic remanent magnetization (ChRM).

125 In the diabase dikes, the Curie temperature of ~570°C indicates the presence of
126 magnetite, with a contribution of maghemite identified by an irreversible decay at around 350°C
127 (Figure 2A). The diabase displays two components of magnetization, better evidenced by
128 thermal (Figure 3C) than by AF demagnetization (Figure 3D). The high-temperature component,
129 which is origin-trending, is unblocked between 400 and 590°C.

130 The magnetic mineralogy of rocks from Victoria Island and Shaler Supergroup is a
131 mixture of pyrrhotite and magnetite. Pyrrhotite is evidenced by significant unblocking
132 temperatures of sIRM around 300-320°C (Figure 2B), and the S_{-300} ratio of -0.79 that indicates
133 the significant contribution of a high coercivity mineral. Pyrrhotite has previously been reported
134 for the Cambrian-Ordovician sedimentary sequence in the region (e.g., *Quesnel et al.*, 2013). The
135 absence of field-dependence of low field magnetic susceptibility suggests a small pyrrhotite
136 grain size (*Worm et al.*, 1993), as classically found in many pyrrhotite-bearing sedimentary rocks
137 (e.g., *Rochette et al.*, 1992). Magnetite is indicated by the significant fraction of the sIRM
138 unblocked above 330°C and up to 580°C (Figure 2B). Among the sedimentary rocks studied for
139 paleomagnetism, 16 out of 21 sites showed unstable remanence during demagnetization and did
140 not provide interpretable results, except for four sites from the Shaler Supergroup and for one
141 site from the Victoria Island formation. These seven sedimentary rocks (dolostones and
142 mudstones) display two components of magnetization, evidenced by thermal demagnetization
143 (Figure 3E-F) where AF demagnetization (not shown) fails to separate both components. The
144 origin-trending high-temperature component is unblocked between 290 and 350 °C (310°C for
145 the only successful Victoria Island site, the remanence being too weak above this
146 demagnetization step).

147

148 **4 Discussion**

149 It is crucial to determine the age of the remanent magnetizations identified in these rocks
150 relative to the impact. The breccia dikes were formed during the impact event and their magnetic
151 remanence would have been acquired both by the clasts and the fine-grained matrix as they
152 cooled following emplacement and associated frictional heating. It has been shown that impact-

153 related tilting occurs quite rapidly, taking place over a timescale shorter than several minutes in
154 mid-sized impact craters (Fairchild et al., 2016). Therefore, the impact breccia is expected to
155 carry a thermoremanent magnetization acquired when the breccia cooled following impact-
156 related tilting. Such a timing of impact acquisition has been shown for clastic breccia dikes
157 within the Slate Island impact structure (Fairchild et al., 2016). However, because frictional
158 heating in the breccia dikes is very localized (Fairchild et al., 2016), the target sedimentary rocks
159 and the diabase dikes may or may not have been remagnetized by the impact.

160 A paleomagnetic tilt test was used to estimate the relative timing of magnetization and
161 impact tilting (Tauxe and Watson, 1994). This test was performed at site levels and not within
162 sites because bedding was almost constant at each individual site. As expected, for all studied
163 lithologies, the low-coercivity / low-temperature components fail the tilt test and were therefore
164 acquired following tilting of the beds. The direction corresponds to the present day local
165 magnetic field such that it is interpreted to be a recent viscous overprint (Figure 4C). For the
166 impact breccia, the tilt test is also negative for the high coercivity components and progressive
167 tilt test indicate a maximum grouping of the directions at 0% untilting. The ChRM of the breccia
168 is interpreted as a full thermoremanent magnetization (TRM) acquired as the breccia cooled
169 shortly after breccia emplacement and impact tilting. For the Shaler Supergroup, the tilt test is
170 also negative, as illustrated by the much larger scattering after tilt correction (Figure 4A-B). Only
171 one site from the Victoria Island formation provided paleomagnetic results suitable for
172 interpretation. The tilt-corrected paleomagnetic direction for this site is compatible with that
173 from the Shaler Supergroup and we considered it as a post-tilting impact related magnetization as
174 well. The possible processes to account for post-tilting remagnetization of these sedimentary
175 rocks are thermal magnetization during cooling from impact-related heating, shock
176 magnetization during pressure release immediately after passage of the impact shock wave, or
177 chemical magnetization resulting from post-impact hydrothermal activity (e.g., Zylberman et al.,
178 2017). Shock remanent magnetization is excluded as the source of the impact-related
179 magnetization because the release of the shock wave occurs before tilting, so that a shock
180 remanence would pass a tilt test. Both partial or total TRM from impact-related heating and
181 chemical remanent magnetization (CRM) from impact-related hydrothermal activities can result
182 in a remagnetization allowing the structure to be paleomagnetically dated (Pilkington et al.,
183 1992). In view of the unblocking temperatures of the natural remanent magnetization (NRM) in
184 the sedimentary rocks (290°C to 350°C), a CRM could be explained by the formation of
185 pyrrhotite during hydrothermal activity (e.g., Osinski et al., 2005). However, because the
186 maximum unblocking temperature of 350°C is slightly higher than the Curie temperature of
187 pyrrhotite (320-325°C), we favor a partial thermoremanent magnetization acquired during post-
188 impact cooling from a peak temperature of 350°C.

189 For the three diabase dikes, the tilt test is inconclusive because the beddings of the
190 intruded sediments are similar for the three sites. The ChRM direction is significantly different
191 (before tilt correction) to the average direction computed from the Shaler Supergroup, Victoria
192 Island formation and impact breccia, suggesting that they have not been remagnetized by the
193 impact (Figure 4B). Their virtual geomagnetic poles (VGPs, after tilt correction) are closer to
194 paleomagnetic poles from other igneous rocks of the Franklin Large Igneous Province (Palmer et
195 al., 1983; Denyszyn et al. 2009) than the impact breccia site VGPs. Poorly developed shatter
196 cones have been described in the diabase dikes (Dewing et al., 2013), implying shock pressures
197 above ~2 GPa during the impact event. Such pressure level is well below the pressure-induced
198 magnetite magnetic transition at 12-16 GPa (Ding et al., 2008). Moreover, the coercivity of

199 remanence of samples from the diabase dikes is 39 mT (our measurements, average of 3
200 samples, one per studied dike), and significant shock remagnetization is also unlikely for
201 magnetite with this range of coercivity of remanence (*Bezaeva et al., 2010*).

202 To test further whether or not the diabase dikes have preserved their primary TRM, we
203 collected 4 oriented cores of the Shaler Supergroup sedimentary rocks that were intruded and
204 baked by the dike, at distances from 3 to 25 cm from the dike wall. In addition to a low
205 temperature viscous component, these samples exhibit four magnetization components
206 unblocked over the following temperature range: between 250 and 345°C, between 345 and 370,
207 between 370 and 450°C, and above 450°C (Table 1, Figure 3G). These components are called A,
208 B, C, D in the following for clarity. Among the three higher temperature components
209 components B and D are identical and close to the reverse polarity ChRM of the diabase dikes
210 (Figure 4C). Component C is antipodal to components B and D. These three components are
211 interpreted as partial TRMs acquired successively during cooling from above 500°C following
212 the diabase dike intrusion. During cooling, the geomagnetic field changed from reverse to
213 normal and back to reverse polarity, leading to the record of antipodal directions D, C, and B
214 successively. Such a record of successive polarity intervals has already been observed in slow
215 cooling sedimentary rocks (e.g., *Rochette et al. 1992*). Component A blocked up to 345°C has a
216 direction different from the other 3 components related to the dike intrusion but undiscernible
217 (before tilt correction) from the other remagnetized Shaler Supergroup directions. It is
218 interpreted as a partial TRM acquired following the impact. This result indicates that the post-
219 impact temperature in these rocks was 345°C, in close agreement with the ChRM peak
220 unblocking temperatures measured in the other Shaler Supergroup sediments within the impact
221 structure. Component A is not recorded in the diabase dikes because these rocks have minimal
222 blocking capacity below 350°C.

223 The impact breccia, Shaler Supergroup formation, and Victoria Island formation all have
224 post-tilting impact-related ChRM. These seven paleomagnetic directions are similar (Figure 4B)
225 and the mean pole calculated from these sites is: 349.3°E, 1.2°N, angular radius of 95%
226 confidence cone $A_{95} = 8.3^\circ$, and Fisher precision parameter $K = 53.3$ (Table 1). The sites may
227 have slightly different magnetization ages due to different blocking temperatures and varied
228 cooling history and as a result may partially average out secular variation. However, the
229 conservative interpretation is that the combined pole represents a snapshot of the paleomagnetic
230 field shortly following impact that does not average out secular variation and should be
231 considered a virtual geomagnetic pole rather than a mean paleomagnetic pole.

232 Comparison of this impact pole with the running mean Apparent Polar Wander Path
233 (APWP) for North America (*Torsvik et al., 2012; Besse and Courtillot, 1991*) shows that it is
234 closest to the 520, 510 and 500 Ma mean paleomagnetic poles (Figure 5).

235 Following 500 Ma, the angular distance of the Tunnunik VGP becomes progressively
236 greater from the geographic poles implied by the running mean poles of *Torsvik et al. (2012)* and
237 the paleogeographic model of *Torsvik and Cocks (2017)* and its modification by *Swanson-Hysell*
238 and *Macdonald (2017)* (Figure 6A). From 410 Ma onward to the present, the angular distance
239 between the Tunnunik VGP and the geographic pole exceeds 45°. Deviations between the
240 geographic pole and a virtual geomagnetic pole are expected to arise through secular variation of
241 the geomagnetic field. However, secular variation of the geomagnetic field typically leads to
242 geomagnetic pole positions that are close to the geographic pole. For example, random draws
243 from the paleosecular variation model TK03.GAD (*Tauxe and Kent, 2004*) for a site at the
244 equator will be within 20° of the geographic pole 90% of the time and within 30° of the

245 geographic pole 95% of the time. The further away an impact VGP is from a pole of a given age,
246 the less likely it is to have formed at that age (see similar discussion in *Hervé et al.*, 2015 and
247 *Carporzen and Gilder*, 2006). In order to estimate the probability of the Tunnunik VGP having
248 arisen through secular variation throughout the Phanerozoic, the approach developed by
249 *Fairchild et al.* (2016) was used: the angular distance between the Tunnunik VGP and the
250 paleopoles is compared to that of VGPs randomly sampled from the TK03.GAD secular
251 variation model (*Tauxe and Kent*, 2004). For this analysis, we simulated 10^5 VGPs from the
252 TK03.GAD model in 10 million year increments at the paleogeographic position of the crater.
253 Seeking to quantify the probability of an angular deviation between the paleopole and the
254 Tunnunik VGP as large as that determined at each of these times (Figure 6A), we calculated the
255 percentage of simulated VGPs that are at this angular distance or greater from the pole (Figure
256 6B and 6C). While the Tunnunik VGP is closest to North America's pole path at *ca.* 500 Ma, this
257 analysis shows that the likelihood of a VGP with the angular distance as large as the deviation of
258 the paleopole of the Tunnunik VGP is greater than 5% at every simulated time during the
259 Ordovician, using the minimum angle given the uncertainty of the VGP. However, given the
260 increasing angular distance of the Tunnunik VGP from Silurian paleopoles (from 420 Ma
261 onward), the likelihood of a VGP at such a distance is less than 5% and continues to be a low
262 probability event all the way to the present. The magnetostratigraphy scale for the 500-420 Ma
263 time interval (e.g., *Hounslow et al.*, 2016), although incomplete, shows multiple reversals and
264 does not allow to better constrain the age of the reverse polarity remagnetization observed at
265 Tunnunik structure.

266 Geologic constraints on the timing of the impact come from the age of early Paleozoic
267 shallow-marine sedimentary rocks within the Tunnunik impact structure. Extensive mapping of
268 the shatter cone distribution at the impact structure reveal the youngest rocks with shatter cones
269 to be those of the Victoria Island Formation (*Osinski and Ferrière*, 2016). Conodont
270 biostratigraphy has revealed an Early Ordovician age (*ca.* 487 to 470 Ma) for the Victoria Island
271 Formation (*Dewing et al.*, 2013; *Dewing et al.*, 2015). Faulting associated with impact crater
272 development extends beyond the central region that contains shatter cones and deforms rocks of
273 the Thumb Mountain Formation (*Dewing et al.*, 2013; *Newman and Osinski*, 2016). Conodonts
274 and a fossil assemblage of crinoids, corals, gastropods, and cephalopods indicate a Late
275 Ordovician age for the Thumb Mountain Formation (*ca.* 458 to 445 Ma; *Dewing et al.*, 2013).
276 Overlying the dolostone of the Thumb Mountain is a poorly exposed dolostone unit that *Dewing*
277 *et al.* (2013) tentatively assigned to the Allen Bay Formation. Further to the northwest on the
278 Arctic Platform at Devon Island, biostratigraphy on carbonates of the Allen Bay Formation have
279 revealed it to have an age that spans from the Late Ordovician into the Silurian (*Thorsteinsson*
280 *and Mayr*, 1987). Mapping of the impact structure has largely left rocks assigned to the Thumb
281 Mountain and Allen Bay Formations undivided (*Dewing et al.*, 2013; *Newman and Osinski*,
282 2016). Currently the most robust constraint on the maximum age of the impact event is that the
283 development of the impact structure led to faulting of the Thumb Mountain Formation and
284 therefore occurred after *ca.* 458 Ma. Regional normal faults taken to have formed in association
285 with Early Cretaceous extension cut across the impact structure were interpreted to indicate that
286 the crater formed before *ca.* 130 Ma (*Dewing et al.*, 2013), but this constraint is rather
287 speculative.

288 The position of the Tunnunik VGP is most consistent with an Ordovician age for the
289 Tunnunik impact. While secular variation of the geomagnetic field naturally results in VGPs that
290 differ from the mean paleopole position, the large angle between the Tunnunik VGP and

291 paleopoles 420 Ma and younger makes a deviation of this magnitude a low probability
292 event (Figure 6). The combined paleomagnetic, stratigraphic and biostratigraphic constraints
293 collectively suggest a Late Ordovician to Silurian age of ca. 430-450 Ma, only shortly after
294 deposition of the youngest impacted sediments.
295

296 **5 Conclusions**

297 This study focuses on constraining the age of the recently discovered Tunnunik impact
298 structure. Paleomagnetic directions obtained from impact breccia and sedimentary rocks from the
299 target sequence indicate the acquisition of a magnetization following impact-related tilting
300 during a reverse polarity interval. In contrast, the diabase dikes intruding these sediments have
301 retained their original magnetization unblocked above 400°C. The comparison of the resulting
302 paleomagnetic pole with the apparent polar wander path for North America shows it to be close
303 to Cambrian poles and strongly suggests a Paleozoic age for the crater. The likelihood of the
304 observed impact direction becomes very small (<5% likelihood) if it was acquired after ca. 430
305 Ma suggesting an age of impact that is older than 430 Ma. Combined with the stratigraphic
306 constraints these data indicate an impact age between 450 and 430 Ma, in the Late Ordovician or
307 Silurian Period, soon after deposition of the youngest impacted sedimentary rocks. This old age
308 opens the possibility that ejecta from the Tunnunik crater may have been preserved in the
309 surrounding basin and may be found in the sedimentary rocks of the Arctic platform.

310 The target sedimentary rocks were remagnetized during post-impact cooling. The
311 preservation of pre-impact magnetization unblocked above 400°C in the diabase dikes, and the
312 constraints from the paleomagnetic results obtained on the Shaler Supergroup sediments baked
313 by the intrusions of the diabase dikes indicate collectively that the peak temperature of the
314 thermal excursion associated with the impact was 350°C at the structural level of the studied
315 rocks.
316

317 **Acknowledgments**

318 This project was partly funded by the French Polar Institute IPEV (Institut Paul Emile Victor).
319 The authors are grateful to the Polar Continental Shelf Project for logistical support. The France-
320 Berkeley Fund initiated collaborative research between J.G. and N.L.S.-H. We thank William
321 Zylberman, Cassandra Marion-Beauchamp, and Racel Sopoco for their help in the field during
322 sampling.

323 **References**

- 324 Ames, D.E., Watkinson, D.H. and Parrish, R.R. (1998), Dating of a regional hydrothermal
325 system induced by the 1850 Ma Sudbury impact event, *Geology*, 26, 447–450.
- 326 Besse, J. and V. Courtillot (1991), Revised and Synthetic apparent polar wander path of the
327 African, Eurasian, North American and Indian plates, and True polar wander since 200 Ma, *J.*
328 *Geophys. Res.*, 96, 4029–4050.
- 329 Carpozen, L. and S.A. Gilder (2006), Evidence for coeval Late Triassic terrestrial impacts from
330 the Rochechouart (France) meteorite impact, *Geophysical research letters*, v.33, L19308, doi:
331 10.1029/2006GL027356.

332 Cockell, C. S., Lee, P., Broady P., Lim, D., Osinski, G., Parnell, J., Koeberl, C., Pesonen, L., and
333 Salminen, J., 2005. Effects of Asteroid and Comet Impacts on Lithophytic Habitats – A
334 Synthesis. *Meteoritics and Planetary Science*, 40, 12, 1-14.

335 Cogné, J.P (2003), PaleoMac: A Macintosh™ application for treating paleomagnetic data and
336 making plate reconstructions, *Geochemistry, Geophysics, Geosystems*, 4, 1, 1007, doi:
337 10.1029/2001GC000227.

338 Denyszyn, S. W., Halls, H. C., Davis, D. W., and Evans, D. A. (2009). Paleomagnetism and U–
339 Pb geochronology of Franklin dykes in High Arctic Canada and Greenland: a revised age and
340 paleomagnetic pole constraining block rotations in the Nares Strait region. *Canadian Journal
341 of Earth Sciences*, 46(9), 689-705.

342 Deutsch A., Schärer U. (1994) Dating terrestrial impact events. *Meteoritics*, 29, 301-322.

343 Dewing, K., Pratt, B.R., Hadlari, T., Brent, T., Bédard, J. and R.H.Rainbird (2013), Newly
344 identified “Tunnunik” impact structure, Prince Albert Peninsula, northwestern Victoria Island,
345 Arctic Canada, *Meteoritics & Planetary Science*, 48, 2, 211-223, doi: 10.1111/maps.12052.

346 Dewing, K., Hadlari, T., Rainbird, R.H., and Bédard, J.H., 2015. Phanerozoic geology,
347 northwestern Victoria Island, Northwest Territories; Geological Survey of Canada, Canadian
348 Geoscience Map 171 (preliminary), scale 1:500 000. doi:10.4095/295530

349 Ding Y., Haskel D., Ovchinnikov S. G., Tseng Y.-C., Orlov Y. S., Lang J. C., Mao H. (2008)
350 Novel Pressure induced magnetic transition in magnetite (Fe₃O₄) *Physical Review Letters*,
351 100, 045508.

352 Fairchild, L.M., Swanson-Hysell, N.L. and S.M. Tikoo (2016), A matter of minutes: Breccia
353 dike paleomagnetism provides evidences for rapid crater modification, *Geological Society of
354 America*, 44, 9, 723-726, doi: 10.1130/G37927.1.

355 Gradstein, F.M., Ogg, J.G. and F.J. Hilgen (2012), On the Geological Time Scale, *Newsletters
356 on Stratigraphy*. 45. 171-188., doi:10.1127/0078-0421/2012/0020.

357 Heaman L. M., LeCheminant A. N., and Rainbird R. H. 1992. Nature and timing of Franklin
358 igneous events, Canada: Implications for a Late Proterozoic mantle plume and the break-up of
359 Laurentia. *Earth and Planetary Science Letters* 109:117–131.

360 Hergarten, S. and T. Kenkmann (2015), The number of impact craters on Earth: any room for
361 further discoveries ?, *Earth and Planetary Science Letters*, 425, 187-192.

362 Hervé, G., Gilder, S.A., Marion, C.L., Osinski, G.R., Pohl, A., Petersen, N. and P.J.Sylvester
363 (2015), Paleomagnetic and rock magnetic study of the Mistastin Lake impact structure
364 (Labrador, Canada): implications for geomagnetic perturbation and shock effects, *Earth and
365 Planetary Science Letters*, 417, 151-163, doi:10.1016/j.epsl.2015.02.011.

366 Hounslow, M.W (2016), Geomagnetic reversal rates following Palaeozoic superchrons have a
367 fast restart mechanism, *Nature communication*, doi: 10.1038/ncomms12507.

368 Jourdan, F., Reimold, W.U. and A. Deutsch (2012), Dating terrestrial impact structures,
369 *Elements*, 8, 49-53, doi: 10.2113/gselements.8.1.49.

370 Newman, J.D. and G.R. Osinski (2016), Geological mapping of the Tunnunik impact structure,
371 Victoria Island, Canadian High Arctic, paper presented at the 47th Lunar and Planetary
372 Science Conference, Houston.

373 Osinski, G.R. and L. Ferrière (2016), Shatter cones: (Mis)understood?, *Sciences advances*, 2, 8,
374 doi: 10.1126/sciadv.1600616.

375 Osinski, G.R., Lee, P., Parnell J., Spray, J. G., Baron, M. (2005) A case study of impact-
376 induced hydrothermal activity: the Haughton impact structure, Devon Island, Canadian High
377 Arctic, *Meteoritics & Planetary Science*, 40, 1859–1877.

- 378 Palmer, H.C., Baragar, W.R.A., Fortier, M. and Foster, J.H. (1983), Paleomagnetism of Late
379 Proterozoic rocks, Victoria Island, Northwest Territories, Canada, *Canadian Journal of Earth*
380 *Sciences*, 20, 1456-1469, doi: 10.1139/e83-131.
- 381 Quesnel, Y., Gattacceca, J., Osinski, G.R. and P. Rochette (2013), Origin of the central magnetic
382 anomaly at the Haughton impact structure, Canada, *Earth and Planetary Science Letters*, 367,
383 116-122.
- 384 Reimold, W.U. and C. Koeberl (2008), Catastrophes, extinctions and evolution: 50 years of
385 impact cratering studies, *Golden Jubilee Memoir of the Geological Society of India*, 66, 69-
386 110.
- 387 Schulte, P. and 40 co-authors (2010), The Chicxulub asteroid impact and mass extinction at the
388 Cretaceous-Paleogene boundary. *Science*, 327, 1214-1218.
- 389 Sodero, D.E. and J.P.J. Hobson, (1979), Depositional Facies of Lower Paleozoic Allen
390 Bay Carbonate Rocks and Contiguous Shelf and Basin Strata, Cornwallis and
391 Griffith Islands, Northwest Territories, Canada. *Am. Assoc. Pet. Geol. Bull.*, 63, 1059-1091.
- 392 Swanson-Hysell, N. L. and F. A. Macdonald (2017), Tropical weathering of the Tacnic orogeny
393 as a driver for Ordovician cooling, *Geology*, doi:10.1130/G38985.1
- 394 Thorsteinsson, R. and U. Mayr. (1987), The sedimentary rocks of Devon Island, Canadian Arctic
395 Archipelago, *Geological Survey of Canada Memoir*, 411, 182.
- 396 Tauxe, L. and D.V. Kent (2004). A simplified statistical model for the geomagnetic field and the
397 detection of shallow bias in paleomagnetic inclinations: Was the ancient magnetic field
398 dipolar? *In* J. Channell, D. Kent, W. Lowrie, & J. Meert (Eds.), *Timescales of the*
399 *Paleomagnetic Field*, 145, 101–116. Washington, D.C.: AGU.
- 400 Tauxe, L. and G.S. Watson (1994), The fold test – an eigen analysis approach, *Earth and*
401 *Planetary Science Letters*, 122, 331-341.
- 402 Torsvik, T.H. and L.R.M. Cocks (2017), *Earth history and palaeogeography*: Cambridge, UK,
403 Cambridge University Press, 311, doi: 10.1017/9781316225523.
- 404 Torsvik, T.H., Van Der Voo, R., Preeden, U., Mac Niocaill, C., Steinberger, B., Doubrovine,
405 P.V., Van Hinsbergen, D.J.J., Domeier, M., Gaina, C., Tohver, E., Meert, J.G., McCausland,
406 P.J.A. and L.R.M. Cocks (2012), Phanerozoic polar wander, palaeogeography and dynamics,
407 *Earth Science Reviews*, 114, 325-368, doi: 10.1016/j.earscirev.2012.06.007.
- 408 Worm, H.-U., Clark, D., Dekkers, M.J. (1993) Magnetic susceptibility of pyrrhotite: grain size,
409 field and frequency dependence. *Geophys. J. Int.*, 114:127-137.
- 410 Zylberman, W., Quesnel, Y., Rochette, P., Osinski, G.R., Marion, C. and J. Gattacceca, (2017),
411 Hydrothermally-enhanced magnetization at the center of the Haughton impact structure?,
412 *Meteoritics and Planetary Science*, 1-19, doi:10.1111/maps.12917.
- 413

414 **Figure and Table captions**

415 **Figure 1.** Location of sampled sites. Color codes indicate the sampled formation. Numbered
416 sites are the ones that provided interpretable paleomagnetic results. The red circle is the proposed
417 limit of the impact structure from Newman and Osinski (2016). The purple contour delineates
418 the area where shatter cones have been found. The background image is an Advanced
419 Spaceborne Thermal Emission and Reflection Radiometer (ASTER) Global Digital Elevation
420 Model (GDEM) Version 2 product. The elevation ranges from 0 (white) to 283 m (black).
421 Except for the regional map on the upper left, coordinates are expressed in meters in the
422 Universal Transverse Mercator (UTM) Zone 12 projection with the World Geodetic System

423 (WGS) 84 datum. For the zoomed-in area (upper right), the background image is to a mosaic of
424 orthophotographic images (Digital Globe Quickbird data).

425 **Figure 2.** Intrinsic magnetic properties of studied rocks. A) Susceptibility versus temperature for
426 a diabase dyke sample (site TUN32, heating and subsequent cooling curves are shown), and an
427 impact breccia sample (site TUN20). B) Thermal demagnetization of sIRM as a function of
428 temperature. The red box indicates the unblocking temperature range of the impact-related
429 magnetization of the target sedimentary rocks. The blue box indicates the unblocking
430 temperature range of the pre-impact magnetization of the diabase dikes. The post-impact
431 temperature excursion is constrained between these two boxes. The Curie temperature of
432 pyrrhotite (325°C) is indicated by the thick vertical line.

433 **Figure 3.** Orthogonal projection plot of stepwise demagnetization data before tilt-correction.
434 Representative samples of the 3 main formations are presented: A-B) Lithic impact breccia, C-D)
435 diabase dike, E) Shaler Supergroup, F) Victoria Island formation. G) Shaler Supergroup
436 formation sample collected 25 cm away from the diabase dike of site TUN32. For clarity the four
437 components of magnetization recorded in this sample and discussed in the text are highlighted by
438 colored arrows.

439

440 **Figure 4.** Equal area stereographic projections. Open (closed) symbols are for upper (lower)
441 hemisphere directions. **A)** Directions of the 24 samples from 4 sites of the Shaler Supergroup
442 sediments before (left) and after (right) tilt correction. The red symbols are the low temperature
443 components (isolated between 280 and 330°C) of the four samples collected within 25 cm of the
444 diabase dike of site TUN32. Blue star is the overall mean direction (samples from site TUN32
445 not included). **B)** Low temperature directions (grey symbols) and ChRM directions for the seven
446 sites from the impact breccia, Shaler Supergroup and Victoria Island formations listed in Table 1,
447 before tilt correction. Also shown is the average ChRM direction for the 3 diabase dikes
448 (square), and the average present day magnetic field (red star). **C)** Directions of the four
449 components of magnetization from the Shaler Supergroup sediments collected within 25 cm of
450 the diabase dike at site TUN32. Also shown is the ChRM direction of the diabase dike at this site
451 (in red).

452

453 **Figure 5.** Comparison of the running mean APWP of Laurentia (*Torsvik et al., 2012*) with the
454 Tunnunik virtual paleomagnetic pole which is the average of the virtual geomagnetic poles of the
455 impact breccia, Shaler Supergroup and Victoria formations sites. Ages of the running mean
456 APWP poles are labeled from the Cambrian to the Early Devonian. The running mean poles are
457 shown with the calculated 95% confidence circle (A95) associated with the mean of studies that
458 fall within a 20 Myr sliding window. The poles for 520, 460, 450, 390, 380, 360 and 350 Ma are
459 shown with no such confidence circle as there are no studies within the sliding window and the
460 position of the pole for that age is the result of linear interpolation by *Torsvik et al. (2012)*.

461

462

463 **Figure 6. A)** Angle between Tunnunik impact VGP and paleopoles as a function of time for the
464 *Torsvik et al. (2012)* APWP, the paleogeographic models of *Torsvik and Cocks (2017)* and its
465 Ordovician modification by *Swanson-Hysell and Macdonald (2017)*. **B)** likelihood for a VGP to

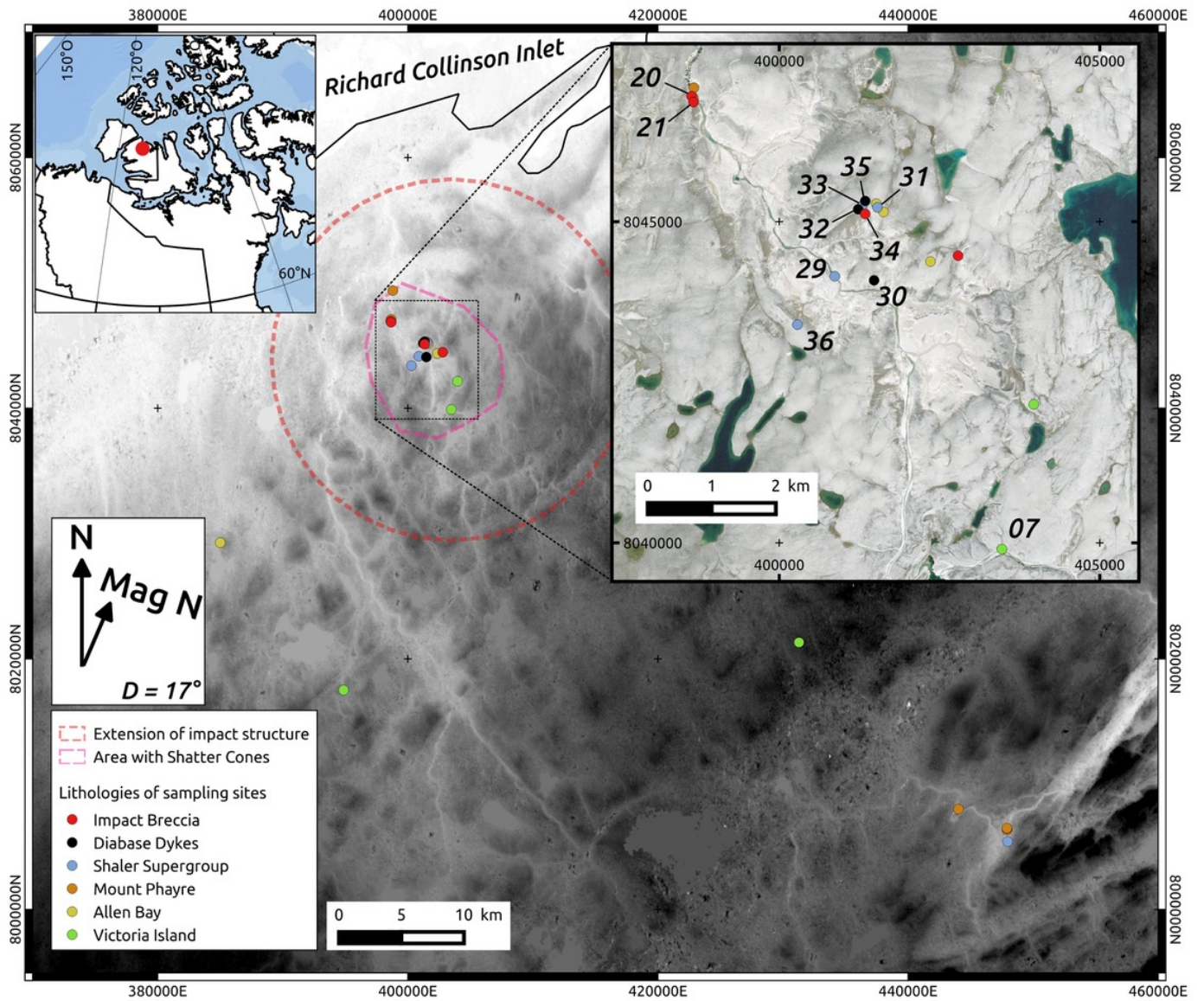
466 occur at an angular deviation from the paleopole equal or greater to that observed for the
467 Tunnunik impact VGP for a Fisherian ($k=20$) distribution of VGPs. **C**) likelihood for a VGP to
468 occur at an angular deviation from the paleopole equal or greater to that observed for the
469 Tunnunik impact VGP for VGPs drawn from the TK03.GAD secular variation model.

470

471 **Table 1.** Site-mean paleomagnetic directions from the Tunnunik impact structure. Site TUN32#
472 is for Shaler Supergroup sediments baked by the diabase dike at site TUN32. These samples
473 have four components of magnetization (A, B, C, D, see text). S_{Lat} and S_{Long} , site latitude and
474 longitude; N/n , number of samples used in the computation of the mean direction / number of
475 samples stepwise demagnetized; ChRM unblocking temperature, the temperature interval of the
476 high temperature component used for calculation; D_g and D_s , declination before and after tilt
477 correction; I_g and I_s , inclination before and after tilt correction; k_g and k_s (noted K_g and K_s for
478 the average of VGPs) precision parameter before and after tilt correction; α_{95^g} and α_{95^s} (noted
479 A_{95g} and A_{95s} for the average of VGPs) are semi-angle of aperture of the cone where the true
480 mean direction lies with 95% confidence before and after tilt correction; Strike, strike of the site;
481 Dip, dip of the site; *, Strike and Dip range from 162/16 to 190/38 (site TUN20), from 213/60 to
482 193/70 (site TUN33); For impact breccia and diabase dikes sites, strike and dip are for the
483 intruded rocks; dp is the semi-axis of the confidence ellipse about the VGP along the great circle
484 path from site to VGP; dm is the semi-axis of the confidence ellipse perpendicular to that great-
485 circle path. NRM, average natural remanent magnetization; χ , average magnetic susceptibility.
486 *The average impact is computed from sites TUN07, 20, 21, 29, 31, 33, 36 (see text).

487

Figure 1



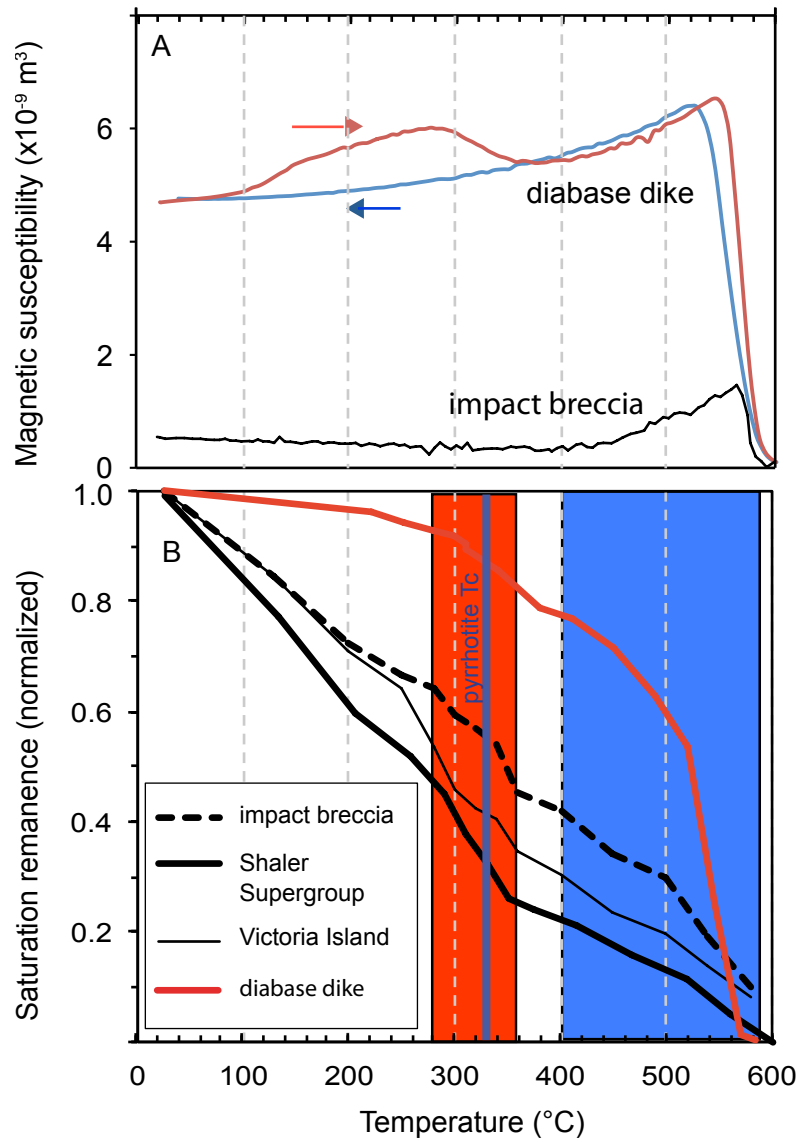
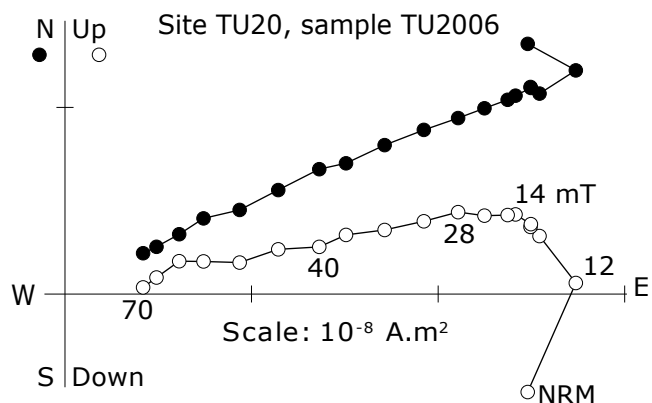
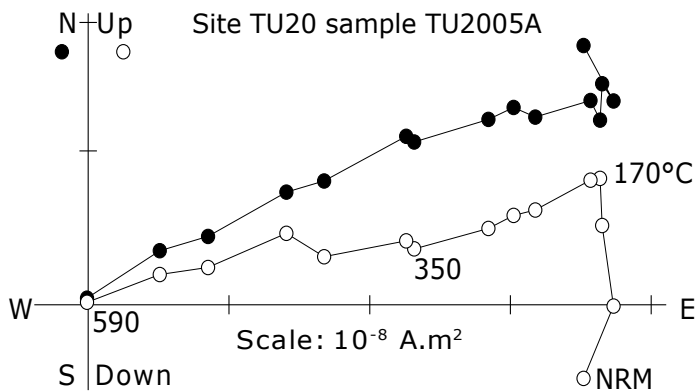


Figure 2

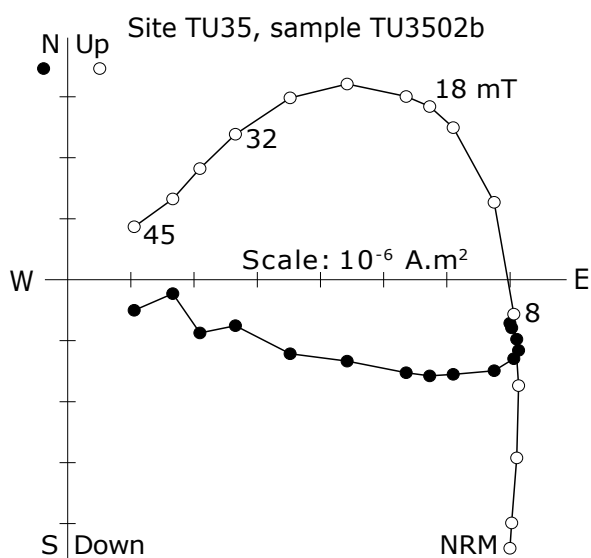
a) Lithic impact breccias, AF demagnetization



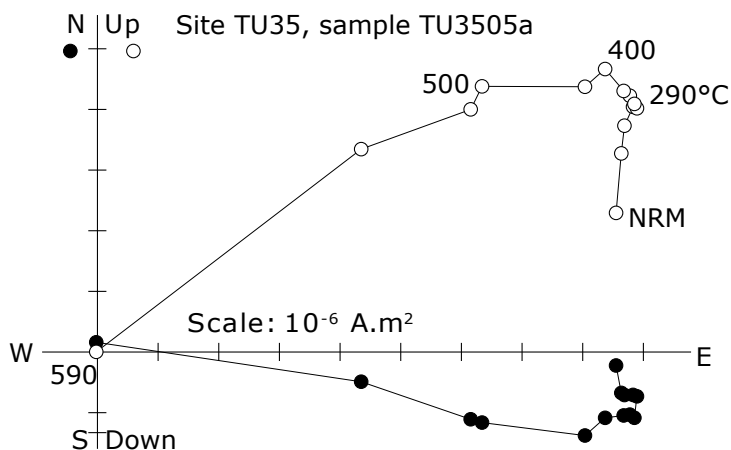
b) Lithic impact breccias, thermal demagnetization



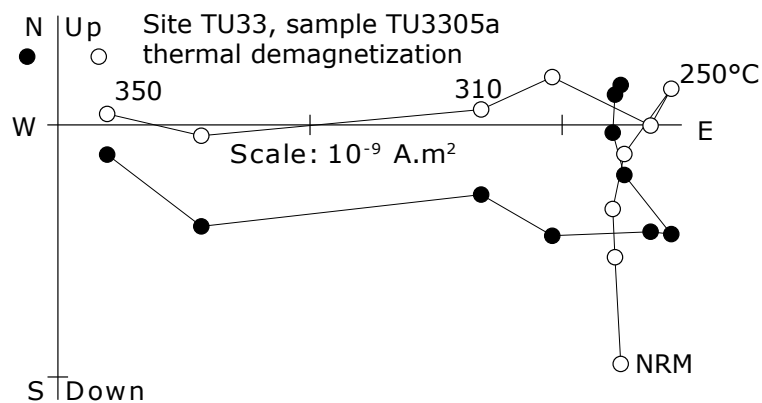
c) Diabase dykes, AF demagnetization



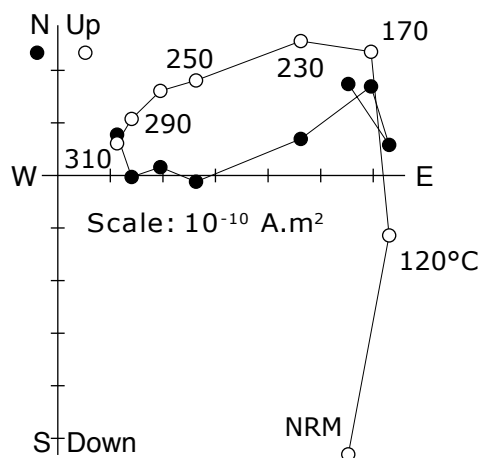
d) Diabase dykes, thermal demagnetization



e) Shaler Supergroup sedimentary rocks



f) Victoria Island sedimentary rocks
Site TUN07, sample TUN0707a
thermal demagnetization



g) Shaler Supergroup sediments baked by diabase dike

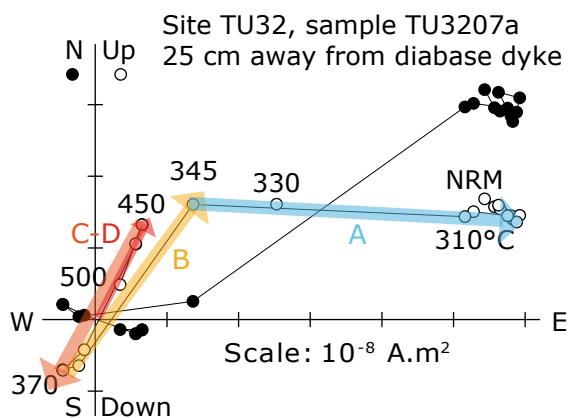


FIGURE 3

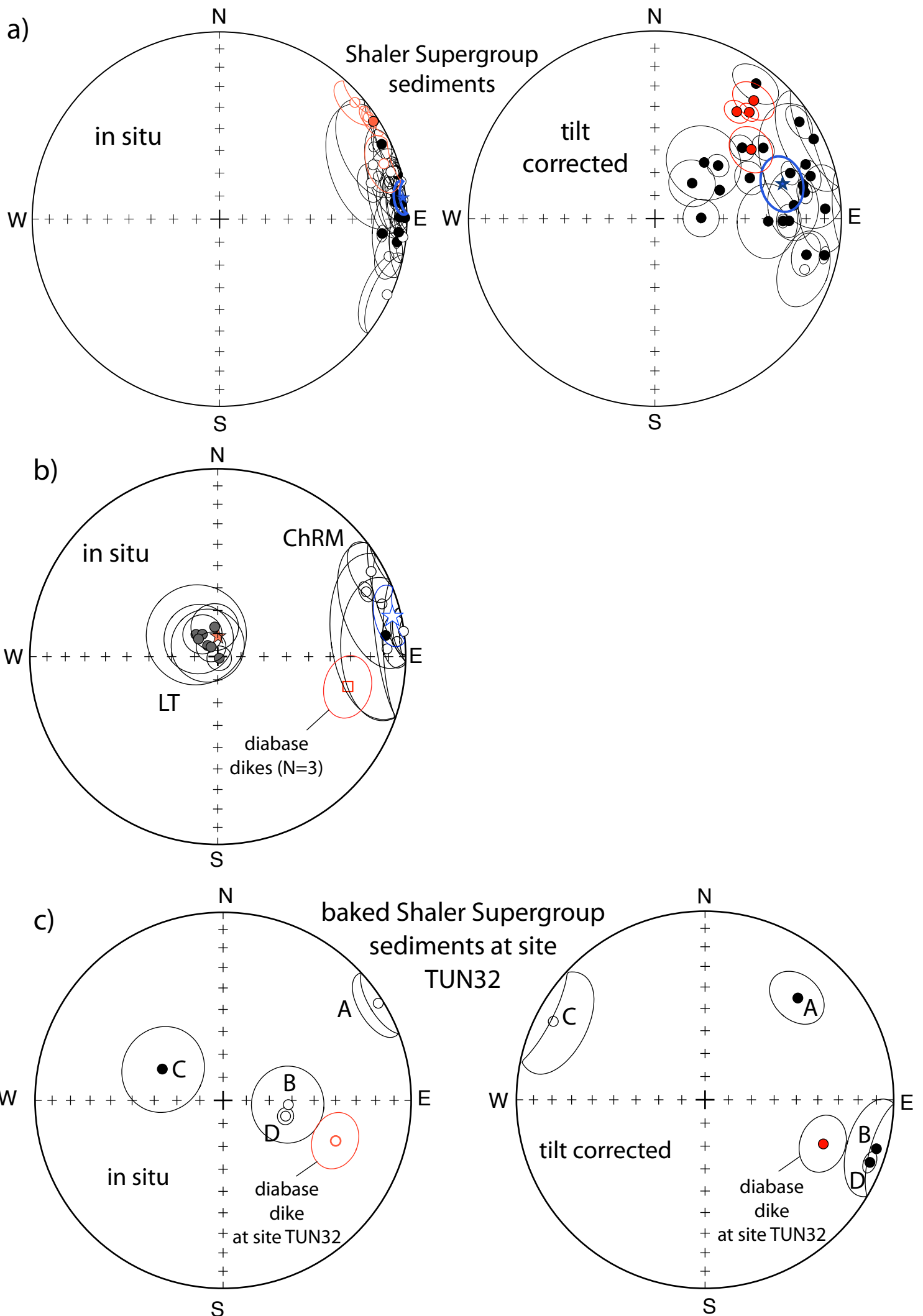


Figure 4

Figure 5

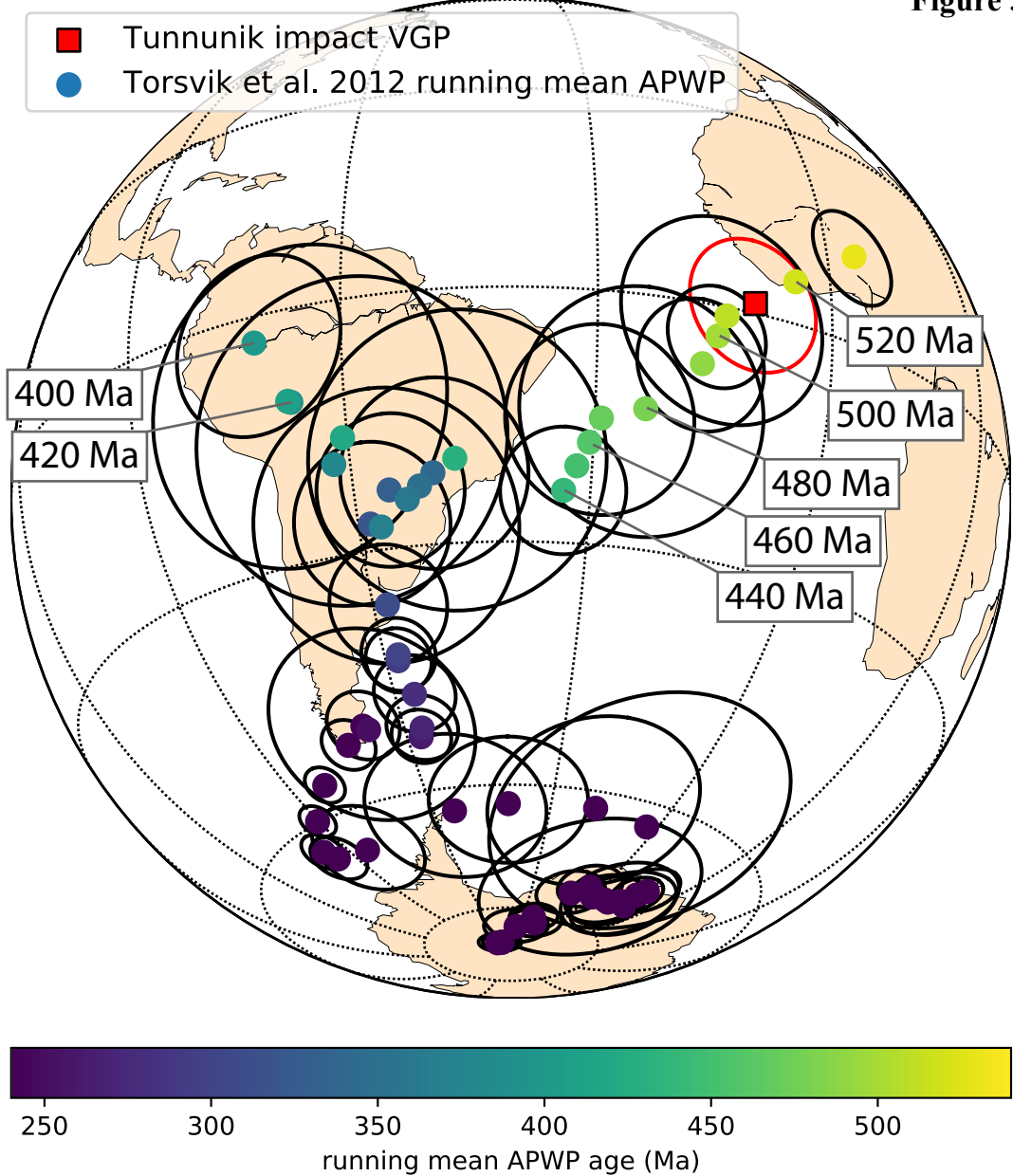


Figure 6

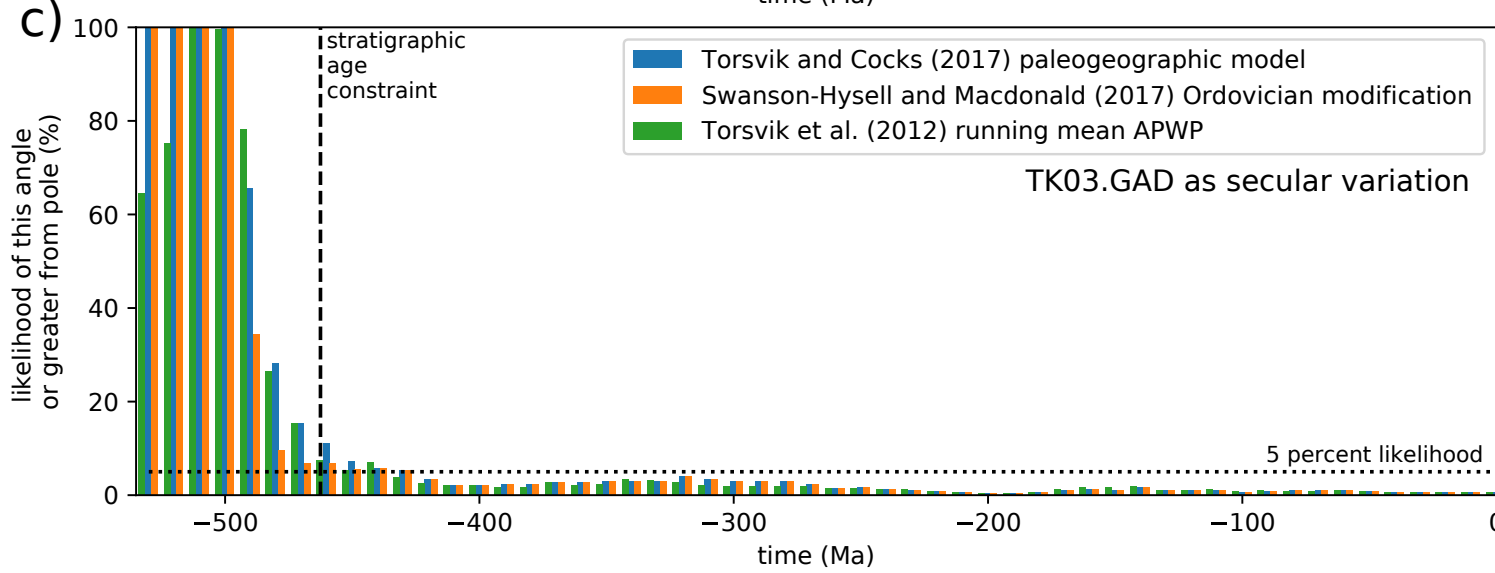
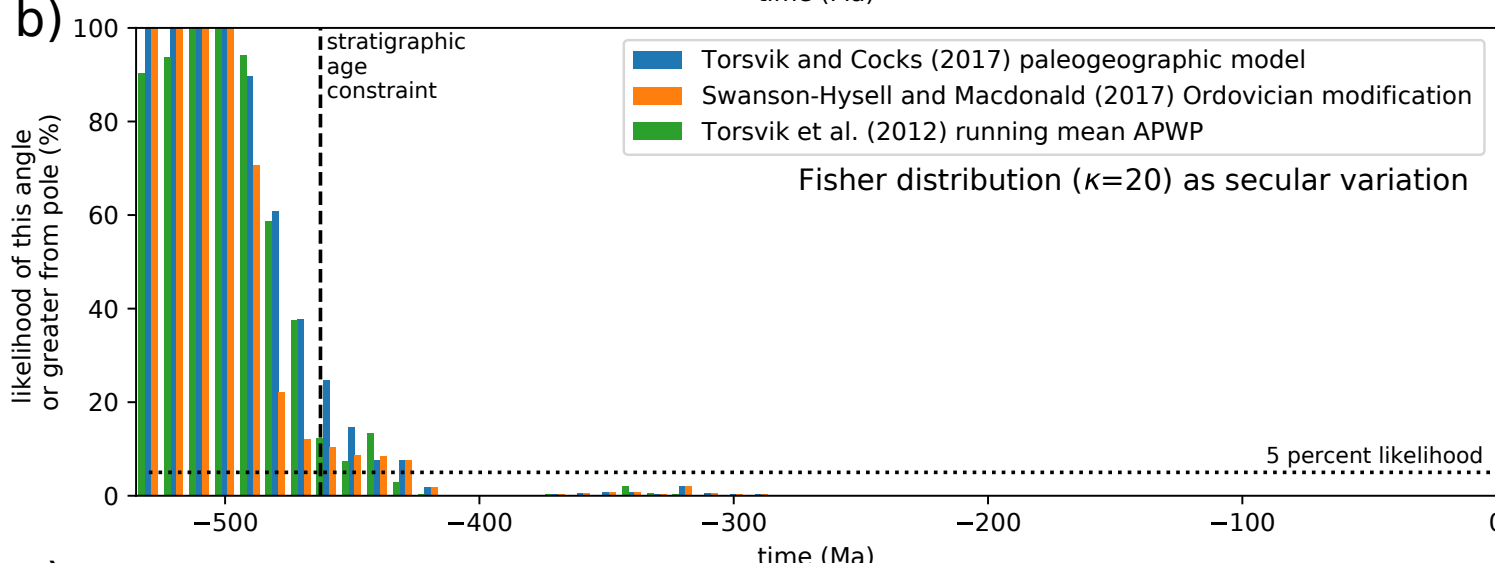
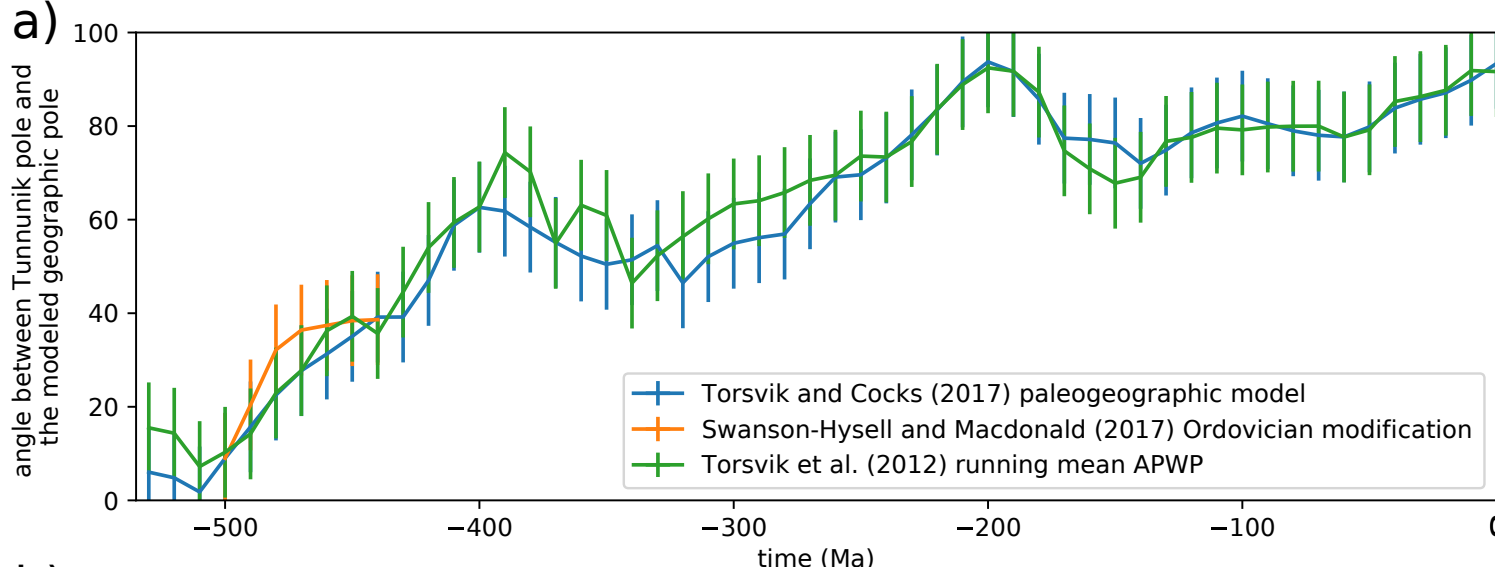


Table 1 - Paleomagnetic results

Formation	Site	Slat (°N)	Slong (°E)	N/n	ChRM unblocking temperatures (°C)	D _g (°)	I _g (°)	k _g	α ⁹⁵ _g (°)	D _s (°)	I _s (°)	k _s	α ⁹⁵ _s (°)	Strike	Dip	Longg (°)	Latg (°)	dp (°)	dm (°)	Longs (°)	Lats (°)	dp (°)	dm (°)	NRM (Am ² kg ⁻¹)	χ (m ³ kg ⁻¹)
Impact Breccia	TUN20	72,4973	-114,0209	15/15	260-590	66,6	-15,2	112,5	3,6	66,9	9,5	67,9	4,7	*	*	0,6	-0,6	1,9	3,7	356,9	11,4	2,4	4,7	9,37E-07	6,61E-08
	TUN21	72,4965	-114,0198	5/5	400-530	61,2	-7,8	51,8	10,7	60,8	15,8	51,8	10,7	162	24	4,8	4,6	5,4	10,8	1,9	16,2	5,7	11	5,11E-07	7,39E-08
Victoria Island	TUN07	72,4363	-113,8668	6/9	250-310	83,1	11,2	6,6	28,1	84,3	12,3	6,6	28,1	95	6	34,1	7,5	14,4	28,5	339,7	7,7	14,5	28,6	2,92E-08	-8,21E-10
Shaler Supergroup	TUN29	72,4732	-113,9503	7/7	270-350	85,4	-5,0	52,4	8,4	85,9	22,3	49,9	8,6	170	28	341,2	-1	4,2	8,4	336,5	12,3	4,8	9,1	2,28E-07	1,08E-08
	TUN31	72,4831	-113,9321	5/5	250-350	72,4	-9,3	13,7	21,5	70,6	20,4	13,7	21,5	194	35	354,2	0,7	10,9	21,7	351,6	15,9	11,8	22,5	9,54E-08	1,72E-08
	TUN33	72,4832	-113,9392	9/9	250-330	82,5	-0,5	50,1	7,3	53,8	46,6	11,1	16,2	*	*	343,3	2	3,7	7,3	2,7	37,1	13,4	20,8	1,32E-07	9,35E-09
	TUN36	72,4662	-113,9665	6/6	230-330	87,6	-10,9	8,7	24,0	81,4	-8,0	8,7	24,0	89	36	340	-4,5	12,3	24,3	345,5	-1,3	12,2	24,2	5,43E-08	2,10E-08
Average impact direction*				7/7		77	-5,5	37,2	10	72,7	17,2	16,8	15,2			349,3	1,2	Kg=53.3	A95g=8.3	350,3	14,3	Ks=27.9	A95s=11.6		
baked Shaler Supergroup	TUN32H-A	72,4827	-113,9410	4/4	200-345	58,6	-3,1	67,3	11,3	42,1	28,3	67,3	11,3	207	70	358,9	55,6	10,7	21,5	14,1	31,3	14,4	24,9	3,99E-06	not measured
	TUN32H-B	72,4827	-113,9410	2/2	345-370	97,3	60,2	190	18,2	297,1	-9,8	190	18,2	207	70	145	47	20,9	27,6	128,7	3,1	9,3	18,4	5,19E-06	not measured
	TUN32H-C	72,4827	-113,9410	4/4	370-450	104,2	-62	654	3,6	111	7,4	654	3,6	207	70	339	-44,9	4,3	5,6	315	-2,6	1,8	3,6	3,99E-06	not measured
	TUN32H-D	72,4827	-113,9410	4/4	450-520	93,8	-61,5	33,3	16,2	106,1	6,4	33,3	16,2	207	70	348,3	-41,4	19,2	24,7	319,8	-1,7	8,2	16,2	3,99E-06	not measured
Diabase dikes	TUN30	72,4729	-113,9320	6/6	465-590	98,4	-32,7	10,8	21,3	98,1	23,2	10,8	21,3	184	56	333,6	-19,5	13,6	24,1	324,8	9,1	12	22,7	2,75E-04	1,14E-05
	TUN32	72,4827	-113,9410	5/6	500-590	110	-35,9	48	11,2	110,2	33,7	48	11,2	207	70	323,1	-24,9	7,5	13	311,5	11,7	7,3	12,7	1,87E-04	9,30E-06
	TUN35	72,4839	-113,9379	8/8	500-590	102,3	-29,6	18,5	13,2	101,5	32,8	18,5	13,2	213	66	329,3	-18,8	8,1	14,6	319,8	12,9	8,4	14,9	2,72E-04	1,62E-05
Average diabase dikes				3/3		103,5	-32,8	194	8,9	103,1	29,6	108,8	11,9			328,7	-21,1	Kg=187	A95g=9	318,7	11,3	Ks=140	A95s=10,5		

Table S1 - list of sampled sites.

Formation	Site	Slat (°N)	Slong (°E)	I/O crater	distance from center (km)	paleomagnetic result
Impact Breccia	TUN20	72,4973	-114,0209	Inside	3,3	yes
	TUN21	72,4965	-114,0198	Inside	3,3	yes
	TUN34	72,4821	-113,9376	Inside	0,5	no
	TUN58	72,4769	-113,8936	Inside	3	no
	TUN12	72,1422	-112,5139	Outside	61	yes
Mafic dikes	TUN30	72,4729	-113,9320	Inside	0,7	yes
	TUN32	72,4827	-113,9410	Inside	0,5	yes
	TUN35	72,4839	-113,9379	Inside	0,7	yes
	TUN17	72,3326	-114,3965	Outside	22,6	no
Allen Bay	TUN50	72,4836	-113,9327	Outside	14,9	no
	TUN51	72,4825	-113,9292	Outside	15,2	no
	TUN56	72,4759	-113,9063	Outside	12,3	no
Clastic unit of Mount Phayre	TUN14	72,1503	-112,5226	Outside	6	no
	TUN15	72,1513	-112,5230	Outside	61	no
	TUN16	72,1516	-112,5232	Outside	61	no
Shaler Supergroup	TUN13	72,1420	-112,5206	Outside	61	no
	TUN29	72,4732	-113,9503	Inside	0,6	yes
	TUN31	72,4831	-113,9321	Inside	0,7	yes
	TUN33	72,4832	-113,9392	Inside	0,5	yes
	TUN36	72,4662	-113,9665	Inside	1,6	yes
Stripy unit of Mount Phayre	TUN21	72,4966	-114,0198	Inside	3,3	no
	TUN22	72,4971	-114,0200	Inside	3,4	no
	TUN23	72,4985	-114,0200	Inside	3,6	no
	TUN28	72,5192	-114,0195	Inside	5,3	no
Tan dolostone unit of Mount Phayre	TUN11	72,1643	-112,6376	Outside	56	no
Victoria Island	TUN03	72,4567	-113,8553	Inside	3,8	no
	TUN07	72,4363	-113,8668	Inside	5,2	yes
	TUN10	72,2800	-113,0234	Outside	38	no
	TUN18	72,2321	-114,0881	Outside	28	no

Site TUN12 is from a 150 m wide mafic dike located 60 km away from the impact structure. Its paleomagnetic direction (D=58°, I=-4°, a95=8.4, k=84, n=5) is different from the three diabase dykes sampled in the impact structure, but this can be easily accounted for by secular variation of the geomagnetic field since the emplacements of these dykes are not necessarily strictly coeval.